Cyclic electric field response of morphotropic Bi1/2Na1/2TiO3-BaTiO3 piezoceramics

M. Hinterstein, L. A. Schmitt, M. Hoelzel, W. Jo, J. Rödel, H.-J. Kleebe, and M. Hoffman

Articles you may be interested in

Polar nanoregions and dielectric properties in high-strain lead-free 0.93(Bi1/2Na1/2)TiO3-0.07BaTiO3 piezoelectric single crystals
J. Appl. Phys. **115**, 014105 (2014); 10.1063/1.4861030

Long ranged structural modulation in the pre-morphotropic phase boundary cubic-like state of the lead-free piezoelectric Na1/2Bi1/2TiO3-BaTiO3
J. Appl. Phys. **114**, 234102 (2013); 10.1063/1.4842855

Domain fragmentation during cyclic fatigue in 94%(Bi1/2Na1/2)TiO3-6%BaTiO3
J. Appl. Phys. **112**, 044101 (2012); 10.1063/1.4745900

Enhanced piezoelectricity and nature of electric-field induced structural phase transformation in textured lead-free piezoelectric Na0.5Bi0.5TiO3-BaTiO3 ceramics
Appl. Phys. Lett. **100**, 172906 (2012); 10.1063/1.4709404

Electric-field-induced strain mechanisms in lead-free 94 % (Bi 1 / 2 Na 1 / 2) TiO 3 – 6 % BaTiO 3
Appl. Phys. Lett. **98**, 082901 (2011); 10.1063/1.3557049

Cyclic electric field response of morphotropic Bi$_{1/2}$Na$_{1/2}$TiO$_3$-BaTiO$_3$ piezoceramics

M. Hinterstein,[1,2] L. A. Schmitt,[2,3] M. Hoelzel,[4] W. Jo,[5] J. Rödel,[3] H.-J. Kleebe,[3] and M. Hoffman[6]

[1]School of Materials Science and Engineering, UNSW Australia, 2052 Sydney, Australia
[2]Institute for Applied Materials, Karlsruhe Institute of Technology, P.O. Box 3640, 76021 Karlsruhe, Germany
[3]Department of Materials and Geoscience, Technische Universität Darmstadt, 64287 Darmstadt, Germany
[4]Heinz Maier Leibnitz Zentrum (MLZ), Technische Universität München, 85747 Garching, Germany
[5]School of Materials Science and Engineering, Ulsan National Institute of Science and Technology, Ulsan 689-798, South Korea
[6]School of Mechanical and Manufacturing Engineering, UNSW Australia, 2052 Sydney, Australia

In this study, the evolution of field induced mechanisms in lead-free piezoelectric ceramics $(1-x)$Bi$_{1/2}$Na$_{1/2}$TiO$_3$-xBaTiO$_3$ with x = 0.06 and 0.07 was investigated by transmission electron microscopy, neutron, and X-ray diffraction. Preliminary investigations revealed a strong degradation of macroscopic electromechanical properties within the first 100 bipolar electric cycles. Therefore, this structural investigation focuses on a comparative diffraction study of freshly prepared, poled, and fatigued specimens. Transmission electron microscopy and neutron diffraction of the initial specimens reveal the coexistence of a rhombohedral and a tetragonal phase with space group *R3c* and *P4bm*, respectively. *In situ* electric field X-ray diffraction reveals a pronounced field induced phase transition from a pseudocubic state to a phase composition of significantly distorted phases upon poling with an external electric field of 4 kV/mm. Although the structures of the two compositions are pseudocubic and almost indistinguishable in the unpoled virgin state, the electric field response shows significant differences depending on composition. For both compositions, the application of an electric field results in a field induced phase transition in the direction of the minority phase. Electric cycling has an opposite effect on the phase composition and results in a decreased phase fraction of the minority phase in the fatigued remanent state at 0 kV/mm. © 2015 AIP Publishing LLC. [http://dx.doi.org/10.1063/1.4922145]

More than sixty years after the discovery of strong and stable piezoelectric effects in lead zirconate titanate (PZT),[1] PZT is still the dominant ceramic for piezoelectric applications. However, a revised ecological awareness all over the world has driven legislation against the continuous use of toxic lead-containing compounds and in favor of lead free materials, which do not raise the same concerns, particularly in regards to potentially toxic by-products during manufacture and disposal. Recently, the European Union revised the two main pieces of legislation addressing these issues: The Directive on waste electrical and electronic equipment (WEEE Directive)[2] and the Directive on the restriction of the use of certain hazardous substances in electrical and electronic equipment (RoHS Directive).[3] These measures sparked the search for sustainable lead-free piezoceramics and resulted in an exponential increase of publications on this topic over the last two decades.[4] Among the various alternative lead-free piezoelectric material systems, bismuth sodium titanate (BNT) based ceramics attracted wide interest in the scientific community as a replacement material for PZT.[4] Especially, $(1-x)$Bi$_{1/2}$Na$_{1/2}$TiO$_3$-xBaTiO$_3$ (BNT-xBT) is an interesting candidate due to high strain at the morphotropic phase boundary (MPB), where a phase coexistence is present.

Takenaka *et al.*[5] reported the existence of an MPB in BNT-xBT at x = 0.06–0.07. Hereafter, these compositions will be labeled BNT-6BT and BNT-7BT. They proposed that in this compositional range, a rhombohedral-to-tetragonal phase transition takes place, which is similar to the MPB in PZT. However, Ranjan and Dviwedi[6] as well as Garg *et al.*[7] suggested a composition dependent rhombohedral to "nearly cubic" structural phase transition at x = 0.06. On the basis of TEM results and dielectric constant measurements a phase diagram for unpoled BNT-xBT was published by Ma and Tan.[8] According to their phase diagram, BNT-6BT belongs to a rhombohedral *R3c* phase, having a complex domain structure. Specimen BNT-7BT was determined to consist of a tetragonal *P4bm* phase with nanodomain morphology.

Structural studies on pure BNT revealed the presence of nanoscale domains with a$^-$a$^-$c$^+$ octahedral tilting.[9] Averaging over several domains yielded an a$^-$a$^-$c$^-$ antiphase tilting.[10] By means of *in situ* transmission electron microscopy (TEM) electric-field experiments, it was possible to determine the evolution of phases as a function of poling field.[11,12] Measurements of the piezoelectric coefficient d$_{33}$ provided a strong correlation between high d$_{33}$ and electric field induced creation of MPBs. An electric-field-induced volume change for BNT-xBT ($0 \le x \le 0.15$) revealed a high amount of axial and radial strain for MPB compositions.[13] Thereby, BNT-6BT was characterized by a small volume change and BNT-7BT featured maximum strain with small amount of irrecoverable strain.

The electric-field induced phase transformation in BNT-6BT was also studied with neutron diffraction by Simons

et al.[14] They demonstrated that the initial system, which can be regarded as a pseudocubic phase with slight tetragonal and rhombohedral lattice distortions, irreversibly transformed to a predominantly rhombohedral modification. The poled sample featured the presence of distorted tetragonal and rhombohedral phases. In addition, Hinterstein *et al.* reported that the giant recoverable strain in $(K_{0.5}Na_{0.5})NbO_3$-modified BNT-xBT arises from a reversible field induced phase transition between the initial pseudocubic structure and the distorted field induced phases.[15]

With high-energy X-ray diffraction, the irreversible electric field induced phase transition in BNT-7BT from initial pseudocubic to tetragonal phase was investigated.[16] Due to a variation in intensity ratio of the 002/200 reflections as a function of the angle between scattering vector and applied electric field, the authors concluded the presence of a remarkable domain texture within the tetragonal phase. Bipolar[17,18] and unipolar[18] fatigue behavior of BNT-6BT were examined with neutron[17] and X-ray[18] diffraction and revealed a continuous decrease in properties, such as polarization, strain as well as ε_{33} and d_{33}, as a function of cycle number.

For actuator fabrication, the understanding of fatigue plays a crucial role in improving materials performance. Several mechanisms,[19,20] like microcracking,[21,22] drift of charge carriers,[23,24] and structural changes,[25] have been reported to contribute to fatigue. This investigation is focused on structural changes caused by electric cycling, which leads to material degradation and thus fatigue. Therefore, in this study structure evolution of the two MPB compositions BNT-xBT with x = 0.06 and 0.07 was investigated by diffraction studies in the initial versus poled and fatigued state.

In the present study, two piezoceramics of the binary system $(1-x)Bi_{1/2}Na_{1/2}TiO_3$-$xBaTiO_3$ with x = 0.06 and 0.07 were investigated using X-ray, neutron, and electron diffraction. A detailed description of the sample synthesis is given elsewhere.[26] Neutron diffraction experiments were carried out at the high-resolution powder diffractometer SPODI at research reactor FRM-II (Garching, Germany)[27] with an incident wavelength of $\lambda = 1.5484$ Å. High resolution X-ray diffraction measurements were performed at the high resolution powder diffraction beamline B2 at HASYLAB (DESY, Hamburg, Germany) with a scintillation counter with an analyzer crystal at an incident wavelength of $\lambda = 0.538$ Å using transmission geometry. For X-ray diffraction, sintered pellets were polished to a thickness of 100 μm. After measuring the initial state, silver electrodes were sputtered on the top and bottom faces of the sample. During *in situ* X-ray diffraction, a maximum voltage of 400 V was applied to the samples, which corresponds to an electric field of 4 kV/mm. Two samples of each composition were fatigued *ex situ* under a bipolar triangular load at the frequency of 50 mHz and a maximum electric field of 6 kV/mm. In order to reach a fatigued state, the samples were exposed to 100 bipolar cycles.

Data analysis was performed by Rietveld refinement with the program packages Fullprof[28] and MAUD.[29] The structure models consisted of a rhombohedral $R3c$ phase and a tetragonal $P4bm$ phase. For the textured, poled samples an exponential harmonics model accounted for the preferred orientation during the refinement.[30] TEM sample preparation

of initial and *ex situ* fatigued specimen included polishing, ultrasonic disc cutting, dimpling, and ion-thinning. TEM experiments were performed on an FEI CM20 (FEI, Eindhoven, The Netherlands) operated at 200 kV.

The results of the TEM investigations of both compositions are depicted in Fig. 1. Bright field micrographs of the initial, unpoled state along the $[130]_C$ zone axis for BNT-6BT (Fig. 1(a)) and BNT-7BT (Fig. 1(b)) show an almost homogeneous contrast. For BNT-6BT several grains featured a core-shell structured contrast, comparable to $K_{0.5}Na_{0.5}NbO_3$ doped BNT-6BT.[31] In BNT-7BT, some grains exhibited domains, as recently reported.[11] The corresponding selected area electron diffraction (SAED) pattern are depicted in the inset of Figs. 1(a) and 1(b). In the following, the subscript C denotes the pseudocubic perovskite unit cell, whereas R denotes rhombohedral and T tetragonal indexing. Both types of superlattice reflections (SR) $\frac{1}{2}$ *ooo* and $\frac{1}{2}$ *ooe*, where *o* and *e* denote odd and even Miller indices,[32,33] are present, even though with different intensities and widths.

The Rietveld refinements with neutron diffraction data of the initial, unpoled structures of compositions BNT-6BT and BNT-7BT are presented in Figs. 2(a) and 2(b), respectively. With the neutron diffraction data, the SR arising from the oxygen octahedral tilting become visible. The insets depict the positions of the $\frac{1}{2}310_C$ and $\frac{1}{2}311_C$ SR. Although a very weak intensity of the $\frac{1}{2}311_C$ reflection is observable for both compositions, the structures could only be refined with a single phase $P4bm$ model. Due to the weak intensity of the SR and the weak lattice distortion, a phase coexistence with $R3c$ could not be established within the refinements. From the atomic positions, the octahedral tilting angle could be calculated to $\omega_T = 2.49(12)°$ for BNT-6BT and $\omega_T = 2.25(11)°$ for BNT-7BT. With 0.009(3)% for BNT-6BT and 0.008(3)% for BNT-7BT the lattice distortions of the unpoled material are small enough to be almost within the error range.

A direct comparison of the two neutron diffraction patterns is depicted in Fig. 3(a). The SR of both compositions is almost exactly the same as already indicated by the tilt angles from the refinements. Close inspection with high resolution X-ray diffraction also reveals only minor differences (Figs. 3(b) and 3(c)). The 111_C reflection of BNT-6BT features a small shoulder which indicates a small fraction of a rhombohedral distorted phase (Fig. 3(b)). However, the intensity is too low to quantify the amount with a refinement.
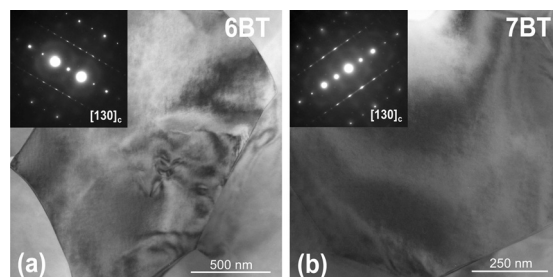

FIG. 1. Bright field (BF) TEM micrograph of (a) BNT-6BT and (b) BNT-7BT in the initial state along pseudo cubic $[130]_C$ zone axis. Corresponding electron diffraction pattern is shown in the inset.
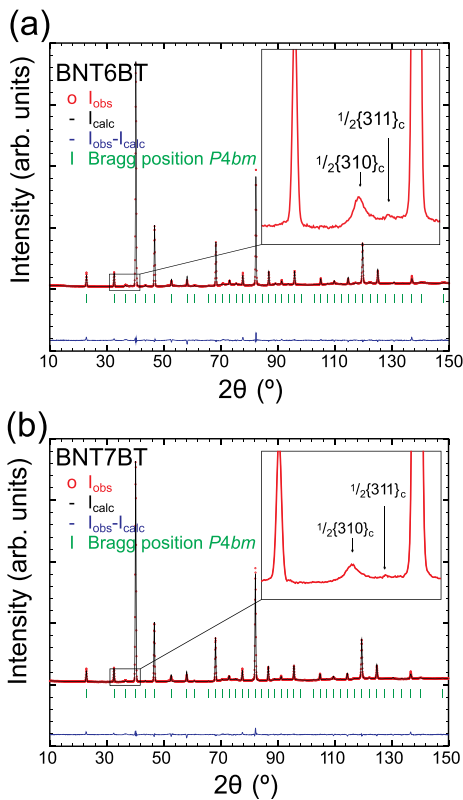
FIG. 2. Rietveld refinement of neutron diffraction data showing the initial structure of (a) BNT-6BT and (b) BNT-7BT. The insets show the $\frac{1}{2}\{310\}_C$ and $\frac{1}{2}\{311\}_C$ superlattice reflections.

FIG. 3. Comparison of (a) the neutron diffraction pattern and (b) and (c) X-ray diffraction pattern of BNT-6BT and BNT-7BT.

The 200_C reflection of the same composition exhibits a small broadening indicating a higher tetragonal lattice distortion (Fig. 3(c)), but with a full width at half maximum (FWHM) of 0.019°, the reflection is still very sharp.

The high resolution X-ray diffraction patterns of BNT-6BT and BNT-7BT revealed the presence of a pseudocubic structure in the unpoled state. The *in situ* measurements were performed in transmission geometry with the electric field parallel to the incident beam ($\psi = 0°$) (Fig. 4). With the application of an electric field of 4 kV/mm, a field induced phase transition takes place. For both compositions, the pronounced lattice distortion can be observed at the 110_C reflection. In addition to the lattice distortion, a texturing can be
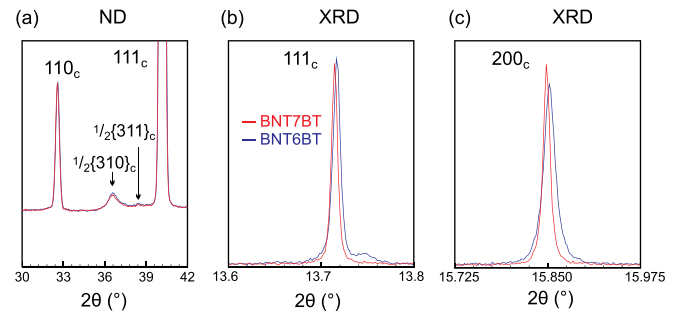
observed (see arrows in Fig. 4). In the remanent state (poled, 0 kV/mm), the texturing is reduced while the lattice distortion is maintained.

Apart from the pronounced splitting of the 110_C reflection, BNT-6BT is characterized by a pronounced splitting of the 111_C reflection and a splitting of the 200_C reflection. Due to a strong texturing, the 111_R reflection almost vanishes (arrow, Fig. 4(a)). The lattice distortions can be calculated as $\eta_T = \frac{c_T}{a_T} - 1$ and $\eta_R = \frac{\sqrt{2}c_R}{2\sqrt{3}a_R} - 1$. A refinement of the lattice parameters reveals a lattice distortion of $\eta_T = 0.244\%$ and $\eta_R = 0.8567\%$ with 16.5% tetragonal and 83.5% rhombohedral phase in the remanent state after poling (0 kV/mm). With applied electric field (poled, 4 kV/mm), a phase transition to 33.8% tetragonal and 64.9% rhombohedral takes place. While the tetragonal lattice distortion changes to $\eta_T = 0.432\%$, the rhombohedral lattice distortion shows no significant change ($\eta_R = 0.8626\%$).

BNT-7BT reveals an opposite behavior. Here, the 200_C reflection provides a significant splitting and strong texturing with an almost vanishing 002_T reflection (arrow, Fig. 4(b)). The 111_C also shows splitting comparable to the 200_C reflection of BNT-6BT. The refinement reveals a lattice distortion of $\eta_T = 1.2656\%$ and $\eta_R = 0.314\%$ with 66.6% tetragonal and 36.4% rhombohedral phase in the remanent state (poled, 0 kV/mm, Table I). Under the influence of an applied field (poled, 4 kV/mm), BNT-7BT shows a phase transition in the direction of rhombohedral symmetry (54.4% tetragonal and 45.6% rhombohedral phase). The lattice distortion of the
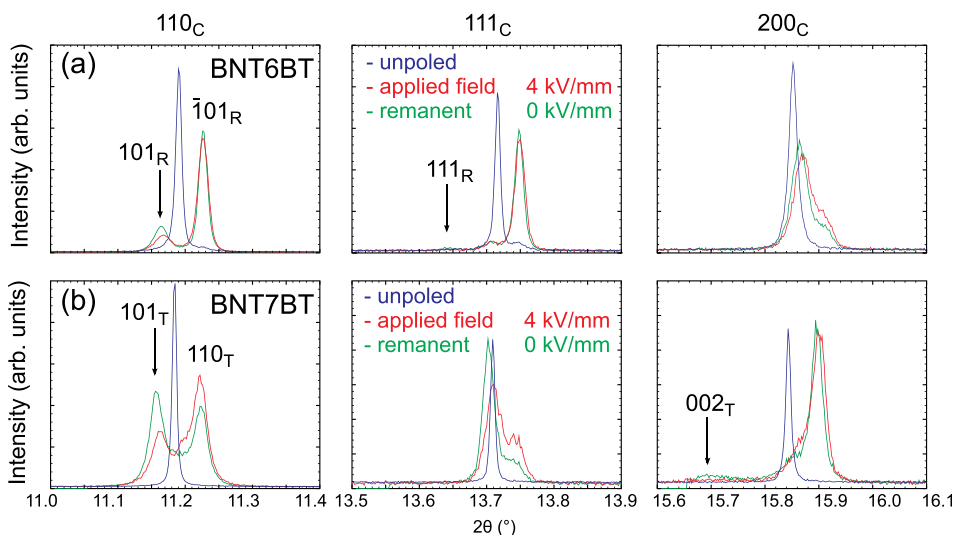

FIG. 4. High resolution X-ray diffraction pattern at $\psi = 0°$ of the remanent state at 0 kV/mm and the applied field state at 4 kV/mm in comparison to the unpoled state of (a) BNT-6BT and (b) BNT-7BT.

TABLE I. Results from Rietveld refinement.

	Structure BNT-6BT		
	Remanent	Field	Fatigued
a_T (Å)	3.89299(7)	3.89234(6)	3.89522(9)
c_T (Å)	3.9025(3)	3.9092(3)	3.90877(10)
η_T (%)	0.244(10)	0.432(9)	0.348(5)
V_T (Å^3)	59.143(7)	59.225(3)	59.307(3)
a_R (Å)	5.50412(2)	5.50444(2)	5.50386(2)
c_R (Å)	6.7733(3)	6.7753(3)	6.7691(4)
η_R (%)	0.8567(10)	0.8626(15)	0.8624(14)
$V_{R(PC)}$ (Å^3)	59.4599(8)	59.4736(11)	59.4548(11)
P4mm (%)	16.5(8)	33.8(7)	16.3(9)
R3m %	83.5(8)	64.9(7)	83.7(9)

	Structure BNT-7BT		
	Remanent	Field	Fatigued
a_T (Å)	3.891630(12)	3.89123(2)	3.891334(12)
c_T (Å)	3.94088(3)	3.94091(5)	3.94138(3)
η_T (%)	1.2656(11)	1.277(2)	1.2862(10)
V_T (Å^3)	59.6838(11)	59.6720(9)	59.682(5)
a_R (Å)	5.51306(9)	5.51201(5)	5.51433(11)
c_R (Å)	6.7733(3)	6.7753(3)	6.7691(4)
η_R (%)	0.314(7)	0.363(5)	0.228(8)
$V_{R(PC)}$ (Å^3)	59.428(5)	59.423(3)	59.419(6)
P4mm (%)	66.6(2)	54.4(3)	64.5(2)
R3m %	36.4(2)	45.6(3)	35.5(2)

rhombohedral phase increases to $\eta_R = 0.363\%$ and to $\eta_T = 1.277\%$ for the tetragonal phase.

Although the two compositions show an almost indistinguishable structure in the unpoled state, BNT-6BT transforms to a predominantly rhombohedral modification under the influence of an electric field, while BNT-7BT transforms to a predominantly tetragonal modification. This is in agreement with the phase diagram, where BNT-6BT is more on the rhombohedral side and BNT-7BT more on the tetragonal side of the MPB.[12,26] With electric field both compositions reveal a phase transition in the direction of the minority phase. In the process the lattice distortion of the minority phase increases significantly compared to that of the majority phase. This behavior is similar to the field induced behavior of actuator materials based on lead zirconate titanate.[34]

When we consider the unpoled sample as a polycrystalline material with pseudocubic structure, all grains have random orientation. The electric field induces either a rhombohedral or a tetragonal phase. While the tetragonal phase offers 6 polarization directions along 001, the rhombohedral phase offers 8 polarization directions along 111. Dependent on grain orientation, one of the phases is favorable concerning the orientation of the polarization vector with respect to the electric field vector. If no other factors would influence the field induced structure, the applied field state should show $\frac{8}{14} = 57.1\%$ rhombohedral and $\frac{6}{14} = 42.9\%$ tetragonal phase. Our results unambiguously demonstrate that both compositions provide a trend towards this phase composition under the influence of an electric field.

After electric cycling, the samples *ex situ* by 100 bipolar cycles, the remanent polarization P_r decreased to 57% and

66% relative to its initial values for BNT-6BT and BNT-7BT, respectively. Fig. 5 displays BF and SAED of specimens (a) BNT-6BT and (b) BNT-7BT in the fatigued remanent state at 0 kV/mm. The presence of domains is visible in both compositions. A recently performed *in situ* electric-field TEM investigation on lanthanum doped BNT-5BT[35] supported the idea of evolving domain configurations as salient features in the fatigue processes.[36] In BNT-6BT, a high amount of grains feature a core-shell structure. Presence of some several nanometer sized pores near to the core region is frequently observed. These pores could act as seeds for the phase transformation, due to a higher local electric field. In BNT-7BT, a homogenous distribution of domains within the grains was observed. The corresponding $[130]_C$ diffraction patterns reveal the presence of both types of SR.

Fig. 6 shows the 110_C, 111_C, and 200_C reflections of the fatigued remanent state at 0 kV/mm in comparison with the remanent state at 0 kV/mm and the applied field state at 4 kV/mm. The strong texturing of the majority phase is still preserved in the fatigued state and can be observed at the 111_R reflection for BNT-6BT and the 002_T reflection for BNT-7BT (see arrows Fig. 6). For BNT-6BT, the strongest reaction to the applied electric field could be observed for the minority phase at the 200_C reflection. While the minority phase fraction (P4mm) increases with electric field, it decreases after fatiguing. The same can be observed for BNT-7BT. Here, also the minority phase (R3m) increases with electric field. After fatiguing, the structure evolves in the opposite direction. The phase fractions from the refinements confirm the observations, although the changes are small (Table I). A comparable tendency could recently be observed for a fatigued actuator material based on lead zirconate titanate.[25] Therefore, for the tetragonal-like material a second phase increases with applied electric field. However, comparing the remanent states at 0 kV/mm, the phase fraction of the field-induced phase is lower after fatiguing for 10^7 cycles. Therefore, it can be considered that the application of a cyclic electric load has, with increasing cycles, an opposite effect on the phase composition compared to applying a single electric field and signifies a fatigue process.

In conclusion, high resolution neutron and X-ray diffraction demonstrated that both investigated compositions, namely, BNT-6BT and BNT-7BT, have similar pseudocubic structure with almost no observable lattice distortion in the initial, unpoled state. However, under the influence of an applied electric field the behavior of the two compositions is different. Both compositions feature a development of strong
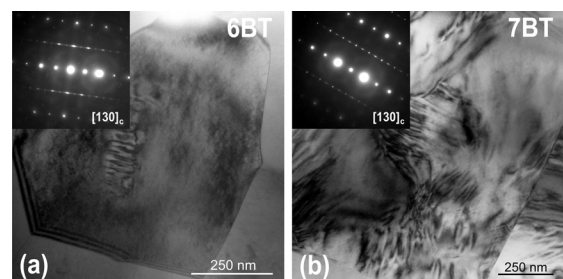

FIG. 5. BF image of (a) BNT-6BT and (b) BNT-7BT after *ex situ* fatiguing. Corresponding electron diffraction pattern along $[130]_C$ is shown in the inset.
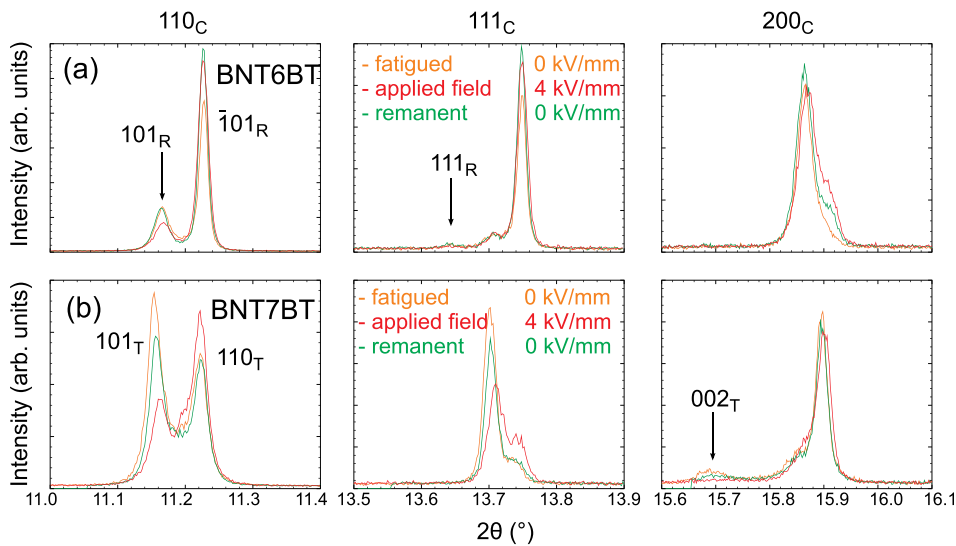
FIG. 6. High resolution X-ray diffraction pattern of (a) BNT-6BT and (b) BNT-7BT of the remanent state at 0 kV/mm and the applied field state at 4 kV/mm in comparison to a fatigued sample at 0 kV/mm at $\psi = 45°$.

lattice distortions during poling. The initial pseudocubic structure transforms to a phase coexistence of distorted rhombohedral and tetragonal phases with preferred orientation. While BNT-6BT provides a strong rhombohedral and a weak tetragonal lattice distortion, BNT-7BT is characterized by a strong tetragonal and a weak rhombohedral lattice distortion. Similar to commercial lead containing piezoceramics,[34] the phase coexistence is the key for the enhanced piezoelectric properties. Additionally, BNT-xBT reveals similar to the lead containing material[25] that cycling has the opposite effect on the phase composition compared to applying a single electric field. Therefore, this study indicates that the phase composition is not only dependent on the chemical composition but also on the state and nature of the applied field state.

[1]B. Jaffe, R. S. Roth, and S. Marzullo, J. Appl. Phys. **25**, 809 (1954).
[2]European Parliament, *Directive 2012/19/EU of the European Parliament and of the Council of 4 July 2012 on Waste Electrical and Electronic Equipment (WEEE)* (2012), pp. 38–71.
[3]European Parliament, *Directive 2011/65/EU of the European Parliament and of the Council of 8 June 2011 on the Restriction of the Use of Certain Hazardous Substances in Electrical and Electronic Equipment (RoHS)* (2011), pp. 88–110.
[4]J. Rödel, W. Jo, K. T. P. Seifert, E.-M. Anton, T. Granzow, and D. Damjanovic, J. Am. Ceram. Soc. **92**, 1153 (2009).
[5]T. Takenaka, K. Maruyama, and K. Sakata, Jpn. J. Appl. Phys., Part 1 **30**, 2236 (1991).
[6]R. Ranjan and A. Dviwedi, Solid State Commun. **135**, 394 (2005).
[7]R. Garg, B. N. Rao, A. Senyshyn, P. S. R. Krishna, and R. Ranjan, Phys. Rev. B **88**, 014103 (2013).
[8]C. Ma and X. Tan, Solid State Commun. **150**, 1497 (2010).
[9]I. Levin and I. M. Reaney, Adv. Funct. Mater. **22**, 3445 (2012).
[10]I. Levin, I. M. Reaney, E.-M. Anton, W. Jo, J. Rödel, J. Pokorny, L. A. Schmitt, H.-J. Kleebe, M. Hinterstein, and J. L. Jones, Phys. Rev. B **87**, 024113 (2013).
[11]C. Ma, H. Guo, S. P. Beckman, and X. Tan, Phys. Rev. Lett. **109**, 107602 (2012).
[12]C. Ma, H. Guo, and X. Tan, Adv. Funct. Mater. **23**, 5261 (2013).
[13]W. Jo and J. Rödel, Appl. Phys. Lett. **99**, 042901 (2011).
[14]H. Simons, J. E. Daniels, W. Jo, R. Dittmer, A. J. Studer, M. Avdeev, J. Rödel, and M. Hoffman, Appl. Phys. Lett. **98**, 082901 (2011).
[15]M. Hinterstein, M. Knapp, M. Hölzel, W. Jo, A. Cervellino, H. Ehrenberg, and H. Fuess, J. Appl. Crystallogr. **43**, 1314 (2010).
[16]J. E. Daniels, W. Jo, J. Rödel, and J. L. Jones, Appl. Phys. Lett. **95**, 32904 (2009).
[17]H. Simons, J. Glaum, J. E. Daniels, A. J. Studer, A. Liess, J. Rödel, and M. Hoffman, J. Appl. Phys. **112**, 044101 (2012).
[18]Z. Luo, J. Glaum, T. Granzow, W. Jo, R. Dittmer, M. Hoffman, and J. Rödel, J. Am. Ceram. Soc. **94**, 529 (2011).
[19]J. Glaum and M. Hoffman, J. Am. Ceram. Soc. **97**, 665 (2014).
[20]Y. a. Genenko, J. Glaum, M. J. Hoffmann, and K. Albe, Mater. Sci. Eng., B **192**, 52 (2015).
[21]Q. Y. Jiang and L. E. Cross, J. Mater. Sci. **28**, 4536 (1993).
[22]M. D. Hill, G. S. White, C.-S. Hwang, and I. K. Lloyd, J. Am. Ceram. Soc. **79**, 1915 (1996).
[23]W. L. Warren, D. Dimos, B. A. Tuttle, R. D. Nasby, and G. E. Pike, Appl. Phys. Lett. **65**, 1018 (1994).
[24]W. Pan, C. F. Yue, and O. Tosyali, J. Am. Ceram. Soc. **75**, 1534 (1992).
[25]M. Hinterstein, J. Rouquette, J. Haines, P. Papet, J. Glaum, M. Knapp, J. Eckert, and M. Hoffman, Phys. Rev. B **90**, 094113 (2014).
[26]W. Jo, J. E. Daniels, J. L. Jones, X. Tan, P. A. Thomas, D. Damjanovic, and J. Rödel, J. Appl. Phys. **109**, 014110 (2011).
[27]M. Hoelzel, A. Senyshyn, N. Juenke, H. Boysen, W. Schmahl, and H. Fuess, Nuclear Instruments **A667**, 32 (2012).
[28]J. Rodríguez-Carvajal, Phys. B: Condens. Matter **192**, 55 (1993).
[29]S. Matthies, L. Lutterotti, and H. R. Wenk, J. Appl. Crystallogr. **30**, 31 (1997).
[30]S. Matthies, J. Pehl, H. R. Wenk, L. Lutterotti, and S. C. Vogel, J. Appl. Crystallogr. **38**, 462 (2005).
[31]L. A. Schmitt and H.-J. Kleebe, Funct. Mater. Lett. **3**, 55 (2010).
[32]A. M. Glazer and O. Ridge, Acta Crystallogr., Sect. B: Struct. Crystallogr. Cryst. Chem. **28**, 3384 (1972).
[33]A. M. Glazer, Acta Crystallogr., Sect. A **31**, 756 (1975).
[34]M. Hinterstein, M. Hoelzel, J. Rouquette, J. Haines, J. Glaum, H. Kungl, and M. Hoffman, Acta Mater. **94**, 319 (2015).
[35]H. Guo, X. Liu, J. Rödel, and X. Tan, Adv. Funct. Mater. **25**, 270 (2015).
[36]J. Glaum, T. Granzow, L. A. Schmitt, H.-J. Kleebe, and J. Rödel, Acta Mater. **59**, 6083 (2011).